Quaternary Science Reviews 239 (2020) 106368

Contents lists available at ScienceDirect

Quaternary Science Reviews

journal homepage: www.elsevier.com/locate/quascirev

Effect of deep Southwestern Subtropical Atlantic Ocean circulation on the biogeochemistry of mercury during the last two glacial/interglacial cycles

Thiago S. Figueiredo [a, *], Thiago P. Santos [a], Karen B. Costa [b], Felipe Toledo [b], Ana Luiza S. Albuquerque [a], Joseph M. Smoak [c], Bridget A. Bergquist [d], Emmanoel Vieira Silva-Filho [a]

[a] Geoscience (Geochemistry) Graduate Program (Environmental Geochemistry), Fluminense Federal University, 24020-141, Niterói, Brazil
[b] Laboratório de Paleoceanografia do Atlântico Sul, Instituto Oceanográfico, Universidade de São Paulo, Praça do Oceanográfico, 191 Cidade Universitária, CEP 05508-120, São Paulo, SP, Brazil
[c] School of Geosciences, University of South Florida, Florida, 33701, USA
[d] Department of Earth Sciences, University of Toronto, Toronto, ON, M5S 3B1, Canada

ARTICLE INFO

Article history:
Received 9 March 2020
Received in revised form
13 May 2020
Accepted 14 May 2020
Available online xxx

Keywords:
Mercury concentration
Paleoproductivity
Atlantic meridional overturning circulation
Organic matter remineralization
Calcium carbonate.dissolution

ABSTRACT

During glacial/interglacial cycles, changes in the strength of the Atlantic Meridional Overturning Circulation (AMOC) modified the intermediate and deep-water mass proportions and high latitude productivity in the Atlantic Ocean. These factors influence the distribution and geochemical partitioning of trace metals in the ocean. Mercury is a redox and productivity-sensitive trace metal, making it a potential proxy of paleoenvironmental changes. Therefore, this work examines the effect of Atlantic Ocean circulation changes during the last two glacial/interglacial cycles on the biogeochemistry of Hg. For this, a high-resolution record of the total Hg concentration was determined in core GL-1090 collected from the Southwestern Subtropical Atlantic that represents the last 185 thousand years. During the reported glacial/interglacial cycles, Hg showed a distinct trend throughout Marine Isotope Stages with higher concentrations during periods of enhanced penetration of northern component water into the southwestern Atlantic. This is supported by the similarity of mercury variability with benthic foraminifera $\delta^{13}C$, suggesting a strong influence of deep ocean circulation on the availability and accumulation of this metal in deep-sea sediments. Mercury geochemistry and particle scavenging were correlated with organic matter (OM) input at the core site. We also noted that mercury responded to redox variation in sediment after Termination II, which can be explained by the increase in deep ocean ventilation due to AMOC strengthening. This hypothesis was confirmed by the antiphase behavior of Hg and Total Organic Carbon when compared with Mn/Al ratios and $CaCO_3$. Our work, therefore, allows for a better understanding of the processes leading to long-term mercury removal to sediments.

1. Introduction

Studies suggest that during the peak of glacial periods, such as during the Last Glacial Maximum (LGM), the composition of deep ocean water masses were dramatically distinct from modern-day (Piotrowski et al., 2008; Skinner et al., 2014). Carbon isotopes ($\delta^{13}C$) from benthic foraminifera, sedimentary $^{231}Pa/^{230}Th$, records of neodymium and silicon tend to indicate a more vigorous penetration of a southern-sourced water mass in the deep Atlantic at times of the glacial expansion with a coeval shallowing of the northern-sourced component (Govin et al., 2009; Negre et al., 2010; Lippold et al., 2012; Griffiths et al., 2013), although nutrient accumulation in the deep ocean might overestimate the degree of such shallowing (Gebbie, 2014; Howe et al., 2016a). The composition of the deep ocean in terms of water mass distribution and nutrient content also plays a critical role in atmospheric CO_2 variability (Lourantou et al., 2010; Sigman et al., 2010; Bereiter et al., 2012). The progressive Atlantic Meridional Overturning Circulation

* Corresponding author.
E-mail addresses: thiagof.bio@gmail.com, thiagofigueiredo@id.uff.br (T.S. Figueiredo).

https://doi.org/10.1016/j.quascirev.2020.106368
0277-3791/

(AMOC) slowdown throughout the glacial period would weaken the vertical mixing between water masses, mainly around the Southern Ocean, enhancing water column stratification, prompting the retention of sequestered carbon in the deep ocean and intensifying $CaCO_3$ dissolution (Yu et al., 2016; Farmer et al., 2019).

Mercury (Hg) is a trace-metal susceptible to abrupt climate change (Martinez-Cortizas et al., 1999; Sanei et al., 2012;Grasby et al., 2013a, b) because Hg and organic carbon cycling are linked. This occurs due to a strong affinity of the Hg for reactive thiol functional groups present in organic matter (Mason and Reinfelder, 1996; Ravichandran, 2004). In the surface waters of the oceans, Hg can be absorbed via scavenging onto organic-rich particles and transported into the deep ocean by the biological pump (Mason and Fitzgerald, 1991; Soerensen et al., 2010; Mason et al., 2012; Lamborg et al., 2014). Therefore, a change in the organic carbon cycle will lead to changes in biogeochemical reactions that influence Hg partitioning in the environment (Sanei et al., 2012; Grasby et al., 2013a, b). A parallel between Hg and biological production was demonstrated in marine sediments from the Pleistocene (Gehrke et al., 2009) and in the Dome C Antarctica ice core during the LGM (Vandal et al., 1993). Kita et al. (2013) proposed a mechanism by which Hg was adsorbed onto OM produced by deep-dwelling species and accumulated in the thermocline when the photic zone was stratified. Kita et al. (2013) went on to state that Hg content and nannoplankton species may be used to determine the extent of ocean stratification and concluded that the photic zone was stratified, which lead to enhanced Hg accumulation in the Caribbean Sea sediments during past interglacials.

Jitaru et al. (2009) noted that the most substantial atmospheric fallout of Hg in surface snow in the Antarctic Dome C region could not be solely attributed to increased biogenic oceanic emission related to an increase in marine productivity and they suggested that dust levels in the Antarctic atmosphere were sufficient to contribute significantly to the irreversible scavenging of atmospheric Hg. A similar correlation between Hg and global atmospheric dust concentration was observed in northeastern Brazil (Fadina et al., 2019). However, factors such as precipitation patterns, runoff events, and sea-level changes also control the input of Hg to the ocean in this region.

In regions of deep-water mass convection, there is greater delivery of Hg toward intermediate and deep depths with subsequent exportation of this metal toward low latitudes regions (Cossa et al., 2011, 2018; Lamborg et al., 2014; Zhang et al., 2014). Based on modeling results there is a robust interocean gradient between the North Atlantic and the North Pacific Oceans with Hg concentration increasing by a factor of 2–3 in the later (Zhang et al., 2014) with the increase attributed to continuous input from the remineralization of sinking particles as the water ages in transit from source regions in the North Atlantic to the North Pacific (Zhang et al., 2014). The interocean gradient of Hg is similar to other biologically essential components such as nitrate, phosphate, silicate, and CO_2 (Zhang et al., 2014).

Despite knowing the carbon cycle and oceanic currents play an important role in Hg distribution and accumulation in the Atlantic Ocean, it is not clear what factors controlled the long-term deep-water Hg accumulation during periods when carbon cycling and ocean circulation were changing the low-latitudes of Atlantic such as over glacial/interglacial cycles. Therefore, we present a high-resolution record of Hg for the last two glacial-interglacial transitions from core GL-1090 (Southwestern Subtropical Atlantic - Santos Basin) using a multiproxy approach to determine controlling mechanisms for Hg accumulation during global climatic transitions.

2. Material and methods

2.1. Study area

Core GL-1090 was collected by the PETROBRAS Brazilian oil company in the Southwestern Subtropical Atlantic (24.92 ◦S, 42.51 ◦W, 2225 m water depth, 1914 cm long) (Fig. 1a). The upper-ocean circulation in the subtropical Southwestern Atlantic is dominated by the southward flowing Brazil Current (BC). The BC originates at ~10 °S latitude from the southern branch of the bifurcation of the South Equatorial Current, which is also the source of the northward-flowing North Brazil Current (Peterson and Stramma, 1991; Stramma, 1991). The intermediate and deep water of the Southwestern Atlantic (600 m and 3000 m) are influenced by Antarctic Intermediate Water (AAIW) and the North Atlantic Deep Water (NADW). The AAIW in the South Atlantic is formed from a surface region of the circumpolar layer, in the northern Drake Passage and the Malvinas Current loop, flowing northward between 600 and 1200 m (Stramma and England, 1999). The AAIW has a salinity ranging between 34.2 and 34.6 with thermohaline limits between 3° and 6 °C (Stramma and England, 1999). The main AAIW salinity minimum at 25°W extends northward from the Subantarctic Front at 45°S (Talley, 1996). The AAIW is also a vertical oxygen maximum in the South Atlantic Subtropical Gyre, reaching an oxygen maximum at the equator along the western boundary and a maximum at only about 20°S in the central and eastern Atlantic (Talley, 1996; Stramma and England, 1999).

The production of NADW is one of the critical variables that determine the Earth's response to climate change, acting to moderate the global redistribution of heat and salt (Dickson and Brown, 1994). The NADW originates in the northern North Atlantic. From about 35°N to 50°S, the NADW is found circulating between 2000 and 4000 m water depth. After 50°S, the thickness of the NADW decreases, reaching a depth of 1000 m in approximately 60°S (Johnson, 2008). It has high salinity and oxygen content with low nutrients (Mémery et al., 2000). Because of the depth of the core (2225 m), there is no significant influence of Antarctic Bottom Water (AABW) for this site in the modern circulation. The intermediate and deep water masses in this region can also be depicted by their distinctive signatures of the carbon isotope ($\delta^{13}C$) of the dissolved inorganic carbon (DIC - $\delta^{13}C_{DIC}$) (Eide et al., 2017a, 2017b). The southern sourced waters masses AAIW and AABW tend to have a lower (<0.75‰) $\delta^{13}C_{DIC}$ that reflects the incomplete nutrient consumption in their formation areas. Otherwise, northern component water NADW splits the southern sourced waters and transports a high (>1.0‰) $\delta^{13}C_{DIC}$ signal until ~ 35 °S (Fig. 1b).

2.2. GL-1090 sampling and age model

For this study, core GL-1090 was sub-sampled at approximately 5 cm resolution. The age model was obtained through a combination of calibrated AMS ^{14}C ages and benthic foraminifera $\delta^{18}O$ tie points aligned to two reference curves (Lisiecki and Raymo, 2005; Govin et al., 2014). Age modeling was based on the software Bacon v.2.2, which reconstructs Bayesian accumulation histories for sedimentary deposits (Blaauw and Christeny, 2011). Details regarding the GL-1090 age model and sedimentation rates (SR) are provided by Santos et al. (2017).

2.3. Total organic carbon (TOC) and calcium carbonate ($CaCO_3$)

For Total Organic Carbon (TOC) analyses, sediment samples of 60 mg were dried, pulverized, and encapsulated in tin foil after removal of carbonate via acidification with 1 M Hydrochloric Acid (HCl). The analyses were performed using a PDZ Europa ANCA-GSL

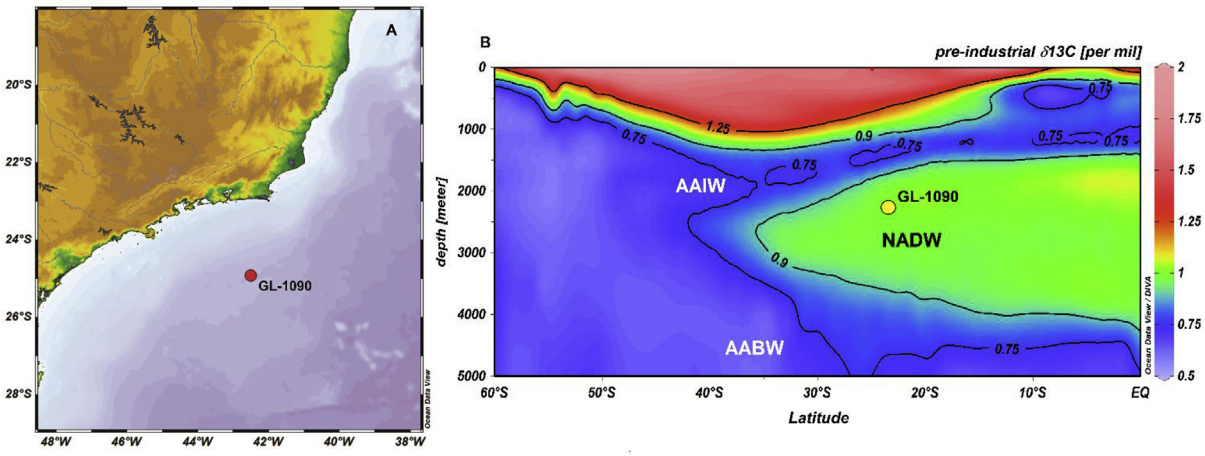

Fig. 1. A: Position of core GL-1090 collected by the Petrobras Brazilian oil company (Santos Basin, 24.92◦S, 42.51◦W, 2225 m water depth, 1914 cm long) in the Southwestern subtropical Atlantic Ocean. B: Pre-industrial distribution of the carbon isotope ($\delta^{13}C$) of the dissolved inorganic carbon (DIC - $\delta^{13}C_{DIC}$) (Eide et al., 2017a; b) for a transect between 0 and 60 °S. Acronyms refer to Antarctic Intermediate Water (AAIW), Antarctic Bottom Water (AABW), and North Atlantic Deep Water (NADW).

elemental analyzer at the Stable Isotope Facility of the University of California, Davis (USA) with an analytical precision of ±0.09%.

Carbonate content was analyzed through the acid-soluble weight loss method (Chaney et al., 1982) . The difference in weight before (Weight 1) and after the attack with HCl (Weight 2) provides a rough estimate of the carbonate content [% CaCO3 =((Weight 1 − Weight 2) × 100)/Weight 1].

2.4. Major elements composition

Titanium (Ti), Aluminum (Al), Iron (Fe), Manganese (Mn) and Calcium (Ca) intensities were obtained by scanning the core surface of the archived half with the X-ray fluorescence Core Scanner II (AVAATECH Serial No. 2) at the MARUM, University of Bremen (Germany). The X-ray fluorescence data were measured every 0.5 cm for GL-1090 by irradiating a surface of approximately 10 mm × 12 mm for 20 s at 10 kV (Venancio et al., 2018). To reduce the dilution effect from sedimentary carbonate, the Fe counts were presented as elementary Fe/Ca ratios, following Govin et al. (2012). Mn was normalized to Al to assess terrigenous contribution over the Mn signal in GL-1090.

2.5. Mercury total concentration

Mercury total concentrations were performed using Zeeman atomic absorption spectrometer RA-915+ with PYRO-915 attachment, following analytical methodology by Sholupov et al. (2004). Freeze-dried sediment (approximately 200 mg) was weighed and placed in a first combustion chamber that reached 680–740 °C. A carrier gas (air) then took the vaporized Hg compounds to a second combustion chamber where the vaporized compounds, including Hg and other interfering compounds, were further decomposed, producing carbon dioxide and water. The rest of the background absorption was eliminated using the Zeeman spectrometer correction. The validation of the method was performed by frequent and simultaneous analysis of sediment standard PACS-2 (n = 10) from the National Research Council – Canada (NRCC). The Hg recovery was 100% with Relative Standard Deviation (RSD) of <5% as the acceptable level of precision. The detection limit was 0.5 ng g^{-1} for 10–400 mg of sediment, and the overall error on Hg was ±5% (1SD).

3. Results

3.1. Age model and sedimentation rates

According to the age model established by Santos et al. (2017), GL-1090 covers the last 185 thousand years, making it possible to identify the last six Marine Isotope Stages (MIS). The average of the sedimentation rate determined from the GL-1090 core was 13 cm/kyr, however, the rates varied considerably. The highest values were found in MIS 4, which reached 24 cm/kyr (Fig. 2f), and the lowest sedimentation rates were observed at approximately 125 ka (MIS 5e) and 11 ka (MIS 2/MIS1) with rates of 2.2 cm/kyr and 2 cm/kyr, respectively (Fig. 2f).

3.2. Total organic carbon and calcium carbonate

TOC concentration ranged from 0.13% to 1.05% with a mean of 0.52% (SD ± 0.1). The lowest value (0.13%) was observed in the transition between MIS 6 and MIS 5e (Fig. 2b). Relative enrichment of TOC occurred during MIS 3, as well as during MIS 5 where the values ranged, respectively, from 0.46% to 0.83% with a mean of 0.60% (SD ± 0.08) and from 0.13% to 0.67% with a mean of 0.54% (SD ± 0.09) (Fig. 2b). However, the MIS 5 sub-stages presented significate oscillations in TOC percentage, mainly between the transition periods (Fig. 2b). In MIS 4, TOC values were relatively low for the entire period with a mean of 0.45% (SD ± 0.05). In the transition between MIS 3/MIS 2, TOC values tended to decrease until the MIS 2/MIS 1 transition, after which the highest values of TOC were observed (Fig. 2b).

Carbonate content ranged from 6.6% to 58.3%, reaching the highest percentages during the transition between MIS 6/MIS 5 (58.3%) and the Holocene (54.3%) (Fig. 2c). The lowest values occurred during MIS 4 and ranged from 18.13% to 29.92% (Fig. 2c). After MIS 4, carbonate content increased significantly and remained high until MIS 1 (Fig. 2c).

3.3. Major element content

The Fe/Ca ratio increased significantly during MIS 6 and early MIS 4 and remained high the entire period (Fig. 2d). Abrupt variations were also observed in MIS 5e/MIS 5d and MIS 5b/MIS 5a transitions (Fig. 2d). The lowest values were found early in MIS 3 up until approximately 16 ka, where there was an abrupt increase

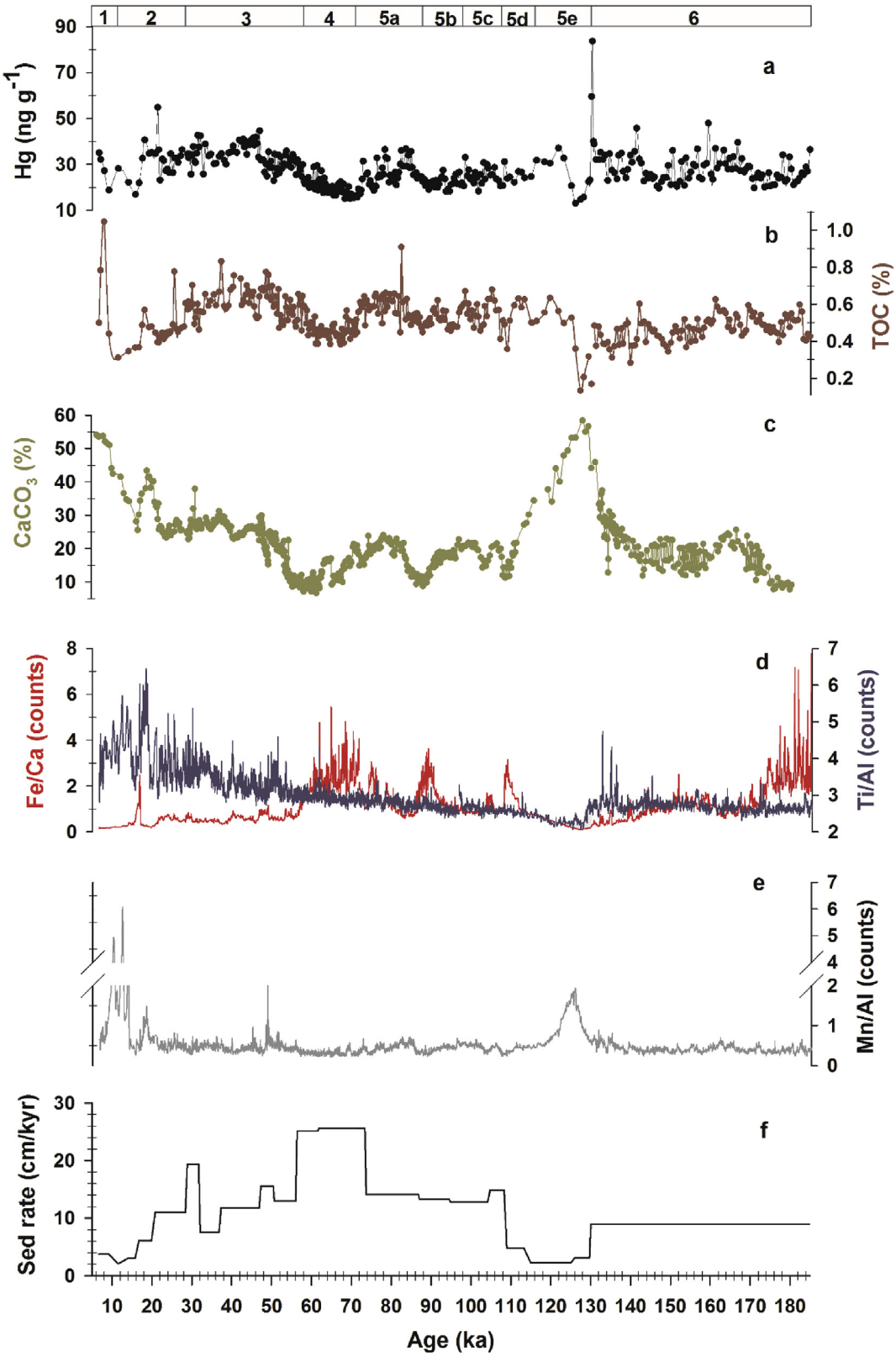

Fig. 2. Distribution of Hg concentration and paleoenvironmental proxies in core GL1090. (a) Hg (ng g^{-1}) (b) TOC (%), (c) $CaCO_3$ (%), (d) Fe/Ca ratio and Ti/Al ratio, (e) Mn/Al ratio, and (f) sedimentation rates (SR) in cm/kyr. Marine Isotope Stages (MIS) boundaries were numbered from 1 to 6 and separated by light grey and white bars.

(Fig. 2d). The Ti/Al ratios showed significant variations in the late MIS 6, MIS 3, and MIS 2, with the most significant variations occurring during MIS 2 (Fig. 2d). The Mn/Al ratios were low and relatively constant throughout most of the core (Fig. 2e). However, during the MIS 6/MIS 5 and MIS 2/MIS 1 transitions, there were abrupt oscillations (Fig. 2e).

3.4. Mercury content

Mercury concentrations ranged from 12.9 ng g^{-1} to 84 ng $g^{-1,}$ and the mean was 27.34 ng g^{-1} (SD ± 8) for all periods (Fig. 2a). The highest Hg values were observed at the MIS 6/MIS 5e transition (129 ka, 83.63 ng g^{-1}) and in the LGM (21 ka, 54.80 ng g^{-1}) (Fig. 2a). The lowest Hg concentrations occurred during MIS 5e when the value decreased to 13 ng g^{-1}. Mercury exhibited a similar pattern to TOC and $CaCO_3$ (Fig. 2a, b, and c), with an exception in the late MIS 6. During MIS 4, Hg, TOC, and carbonate tended to decrease (Fig. 2a, b, and c). The opposite behavior was observed in the Fe/Ca ratios (Fig. 2d) and sedimentation rate (Fig. 2f).

4. Discussion

4.1. Sources and transport of mercury in Southwestern Subtropical Atlantic through glacial/interglacial cycles

Enhancement of the Hg atmospheric input on a global scale has been attributed to an increase of dust load during cold climatic stages and continental runoff (Jitaru et al., 2009; Lacerda et al., 2017; Fadina et al., 2019). However, Hg records in GL-1090 cannot be explained by the mentioned processes. First, Hg in GL-1090 core presented a different pattern concerning Hg records in the Antarctic zone and northeastern Brazil (Fig. 3b) (Jitaru et al., 2009; Fadina et al., 2019). Second, Hg in GL-1090 did not accompany the increase of the dust concentration in the Antarctic zone (Fig. 3a and b). Although Hg in GL-1090 showed an increase during LGM, this variation was low when compared to dust and Hg concentration oscillation in the Antarctic zone (Fig. 3a and b). Third, Fe/Ca ratio and Hg concentration in GL-1090 displayed an inverse pattern (Fig. 3b and c) with Hg concentration negatively correlated to the major elements (Table 1). Therefore, overall Hg distribution in Southwestern Subtropical Atlantic, as recorded in core GL-1090, does not appear to be influenced by increased continental runoff as described by Fadina et al. (2019) for the Brazilian equatorial margin (Fig. 3b).

The Hg/TOC ratio was used to remove the variations in the scavenging effect on the Hg content in the sediments. In this way, it is possible to assess the processes related to the provenance of this metal (Grasby et al., 2013a, b, 2017). An abrupt variation was observed during the MIS 6/5 transition (130 ka) (Fig. 3d). A similar configuration was observed, but with less intensity, during the LGM (Fig. 3d). This variation in the Hg/TOC ratio could be associated with changes in the provenance of Hg, as suggested in Grasby et al., (2013a, b, 2017).

The Ti and Al are derived from aluminosilicates, which are primarily delivered to the oceans via riverine discharge (Arz et al., 1998; Perez et al., 2016). Considering that the distribution of Ti (heavy minerals) in deep-sea sediments is affected by changes in the grain size variation, it has been suggested that variations of the Ti/Al ratio predominantly indicate changes in weathering in source regions (Govin et al., 2009; Muratli et al., 2010).

The Ti/Al ratio from GL-1090 increased in the late MIS 6 and during the LGM. Thus, the rough variation in Hg/TOC could be associated with rapid and episodic events of the terrestrial/riverine Hg transport to this region (Fig. 3c and d). A possible source of Hg to the GL-1090 area would be sediment suspend from the Plata River discharge. According to Govin et al. (2009), Ti/Al values from Plata River sediment have similar values of the surface sediments off south Brazil and Uruguay between 24°S and 38°S. Using Pb isotope Mahiques et al. (2008) established that Plata Pluma water reaches up to 28°S. Therefore, the GL-1090 area would be under the influence of Plata Pluma water and might explain the Hg peak in LGM. However, for late-MIS 6, the Hg/TOC ratio variations are temporally more significant, and Hg/TOC peak was not coupled with Ti/Al ration. Thus, it indicates that other factors such as post-depositional changes could have affected sedimentary geochemistry of Hg in Southwestern Subtropical Atlantic during this period.

Mercury data from GL-1090 was correlated with organic-rich particles during the latest 185 ka (Table 1). This close relationship between Hg and TOC could be confirmed by the Hg/TOC ratio, which was steady most of the time. The Hg concentrations in marine sediments usually reflect the scavenging process by organic particles that occurs in the surface ocean (Mason and Fitzgerald, 1991; Laurier et al., 2004; Zhang et al., 2014). It is estimated that 70% of Hg in thermocline/intermediate water is removed through the scavenging processes by organic-rich particles (Zhang et al., 2014). Lamborg et al. (2016) detailed the vertical transfer of Hg in the ocean and found that the downward flux of this metal supports regenerative scavenging, rather than reversible scavenging, with a balance between adsorption, remineralization, and loss from the water column by sinking.

Although particle sinking from the surface ocean has been described as the primary mechanism for the transporting Hg to deep waters (Mason et al., 1998; Mason and Sullivan, 1999; Laurier et al., 2004; Zhang et al., 2014), GL-1090 data suggest that Hg was not driven by local marine productivity. In MIS 4, the low values in Hg concentration and TOC % did not reflect the high surface productivity found by Costa et al. (2016). In contrast, during LGM, paleoproductivity proxies in GL-1090 (Lessa et al., 2017) and GL-74 (21°15′22.5″ S, 40°02′36.2″ W; water depth of 1279 m, 1975 cm long) (Portilho-Ramos et al., 2015) demonstrated low productivity with an increase only in MIS 5.

According to Laurier et al. (2004), there is a difference in deep Hg concentration between the North Atlantic and the North Pacific Ocean. This occurs due to removal processes involving the Hg in the deep ocean as water moves from the Atlantic to the Pacific Ocean. The inter-ocean Hg fractionation and distribution (Laurier et al., 2004) was also observed by Cossa et al. (2011) in which Hg concentration measured in Circumpolar Deep Waters (CDW) (depths ranging from 500 to 3000 m, far to the East 140°E and South 46–62°S) was lower than Hg concentration measured in NADW. Biogeochemical modeling showed by Zhang et al. (2014) predicted that the progressive increase in Hg concentrations during the transit of deep water from the North Atlantic to the North Pacific was similar to the behavior of biologically active tracers. This supports the idea about the scavenging of Hg in deep waters during their transport poleward.

The $\delta^{13}C$ of C. wuellerstorfi is widely used as a deep-water paleocirculation and paleoproductivity proxy, since carbon isotopic composition from benthic foraminifera exhibits a consistent correlation with the isotopic composition of the DIC from the water mass (Curry and Oppo, 2005; Tessin and Lund, 2013). Thus, more negative values would be related to the presence of water masses containing a higher amount of respired carbon. The Hg curve had a similar pattern to the $\delta^{13}C$ of Cibicides wuellerstorfi from GL-1090 (Santos et al., 2017) (Fig. 4a and d). This relation might explain the source of the metal in GL-1090, which was derived from the global atmospheric pool and followed regenerative deep carbon cycle during its transit as propose by Mason et al. (1998); Laurier et al. (2004); Fitzgerald et al. (2007); Cossa et al. (2011); Lamborg et al. (2016); Cossa et al. (2018).

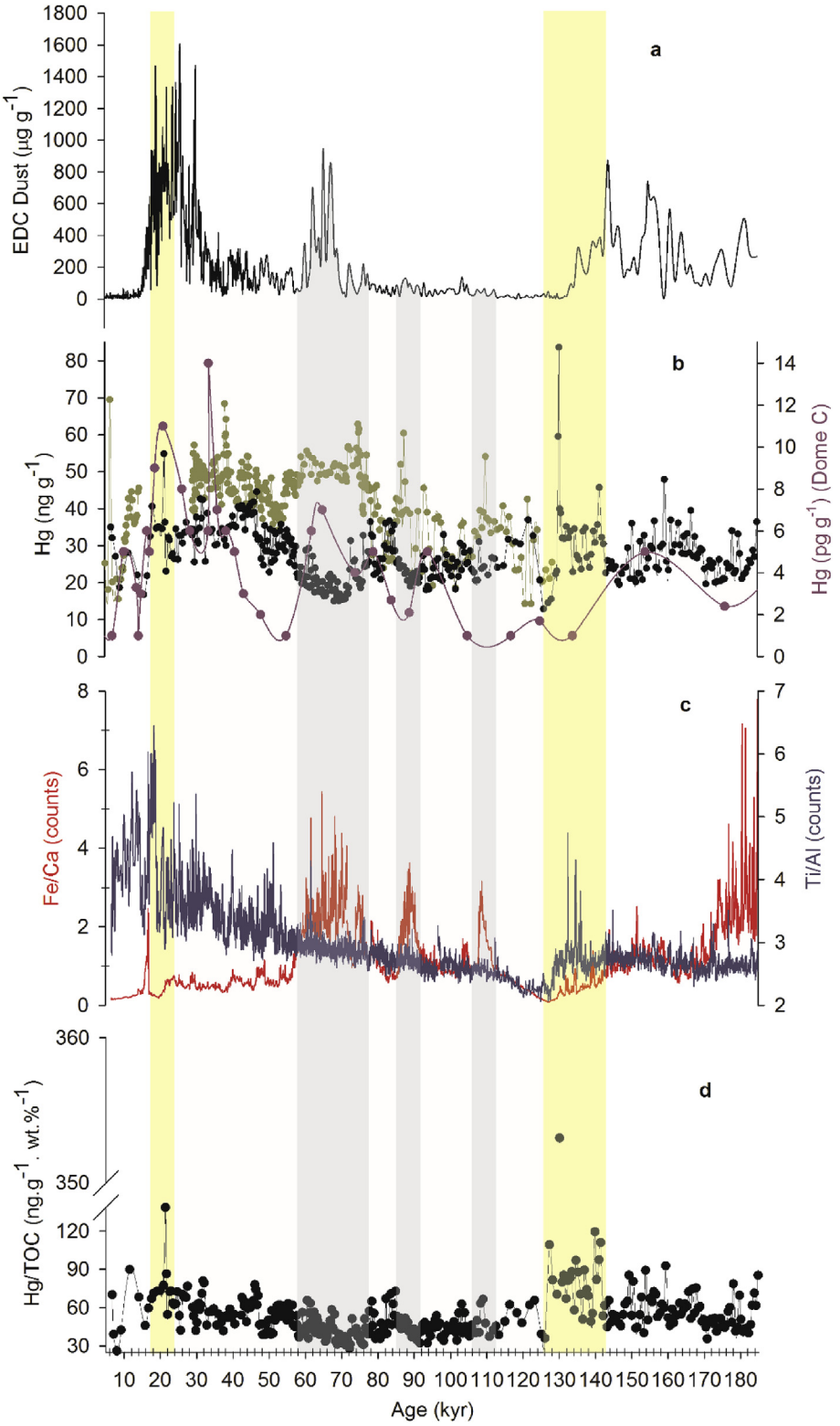

Fig. 3. Relationship between the Hg/TOC ratio and eolian and continental proxies. a) EPICA Dome C ice core record of atmospheric dust deposition in the black line (Lambert et al., 2008). b) Hg (ng g^{-1}) from GL-1090 core in black circles, marine core GL-1248 (0°55.2′S, 43°24.1′W) in dark yellow circles (Fadina et al., 2019) and Hg concentration from Antarctica (Jitaru et al., 2009) in dark pink circle. c) Fe/Ca ratio (red line) and Ti/Al ration (dark blue line) from GL-1090. d) Hg/TOC ratio (black circle) from GL-1090. Light yellow bars represent the additional input of Hg and the relation to change in the diameter of the particle. The light blue bars represent the increase of terrestrial material, and its the relation with Hg loading. (For interpretation of the references to colour in this figure legend, the reader is referred to the Web version of this article.)

Table 1
Spearman rank correlation coefficients for Hg (ng g^{-1}), TOC (%), and major elements in GL-1090. Correlations significant at the 95% confidence level are in bold text.

Variables	Hg	TOC	Fe	Al	Ti	Mn
TOC	**0.55**					
Fe	**−0.69**	−0.37				
Al	**−0.63**	−0.28	**0.84**			
Ti	**−0.65**	−0.31	**0.88**	**0.96**		
Mn	−0.18	0.01	0.12	0.28	0.25	

4.2. Deep ocean mercury cycle and regenerative organic and inorganic carbon processes

Glacial periods are characterized by a strong chemical contrast developed in $\delta^{13}C_{DIC}$ between southern-sourced and northern-sourced component deep waters (Sigman et al., 2010; Ziegler et al., 2013). This likely occurred due to biological pump strengthing in regions of deep-water convection that resulted in the $\delta^{13}C_{DIC}$ increasing in the surface ocean. Additionally, the decrease in NADW production following the advance of glacial climate resulted in a decrease of the vertical mixing between water masses, which enhanced storage of remineralized carbon in the deep-water and produced a further CO_2 drawdown and low $\delta^{13}C_{DIC}$ (Lund et al., 2011; Jaccard et al., 2016; Yu et al., 2016) (Fig. 4f). The $\delta^{13}C$ of C. wuellerstorfi in core GL-1090 shows a very similar pattern with other benthic $\delta^{13}C$ data from the South Atlantic (Jonkers et al., 2015), which indicates that it reflects basin-wide process associated with changes in the South Atlantic ventilation (Fig. 4d).

A similar pattern between Hg concentration, TOC (%), and the $\delta^{13}C$ of C. wuellerstorfi (Fig. 4a, b, and d) suggests that changes in the deep South Atlantic circulation might have played a role in regenerative organic matter cycle and consequently in the availability of Hg in the water column. This is further supported during the MIS 5/MIS 4 transition when GL-1090 data are compared with the εNd data (Fig. 4e).

The chemical composition of the rare earth elements and εNd in oceans results from continental crust weathering and exchanges with seawater along continental margins. (Frank, 2002; Pearce et al., 2013). These processes produce an εNd signature that is relatively less radiogenic for NADW (−13.5) (Piepgras and Wasserburg, 1982), reflecting the ancient continental crust that surrounds its source areas. This value differs from that of the Southern Ocean (εNd = −9 to −8) (Amakawa et al., 2013), which reflects a mixture with more radiogenic Pacific Ocean waters due to young rocks derived from the mantle that surrounds the region.

The Hg concentrations, TOC (%) and $\delta^{13}C$ of C. wuellerstorfi, showed an abrupt decline in their values from late MIS 5 to MIS 4, while εNd had higher radiogenic values (MIS 4) (Fig. 4a, b, d and e). It suggests a lower penetration of the northern component NADW and a greater contribution of corrosives southern water masses (Piotrowski et al., 2005; Griffiths et al., 2013; Jonkers et al., 2015). The presence of more corrosives southern water masses can also be supported by the substantial reduction in the percentage of $CaCO_3$ (Fig. 4c) observed in core GL-1090. This significant drop in $CaCO_3$% could be explained by the increase in the concentration of DIC in deep waters, which enhanced deep waters corrosivity, dissolving $CaCO_3$ and rising the alkalinity (Sigman et al., 2010; Yu et al., 2016; Farmer et al., 2019). This way, enhancement of water-column stratification increased the remineralization of organic matter intensifying the regenerative scavenging of Hg, as described by Lamborg et al. (2016). The intensification of regenerative scavenging would increase the release and storage of Hg(II) species in deep-water. This fact could explain the decrease of Hg concentration in sediment during MIS 4 (Fig. 5).

During the transition between MIS 4/MIS 3, an increase in Hg concentrations was observed while the same trend was observed in TOC, CaCO3, and C. wuellerstorfi δ13C (Fig. 4a, b, and c). MIS 3 is considered an unsettled period with abrupt and repeated millennial-scale oscillations, alternating between cold stadial and warm interstadial events (Kissel et al., 1999; Gutjahr et al., 2010; Hessler et al., 2011). In the North Atlantic, sedimentary records indicate an increase in NADW advection and renewal of AMOC convection during interstadial events (Henry et al., 2016; Rasmussen et al., 2016). Therefore, this may suggest that during the MIS 3, a vigorous NADW associated with the interstadial conditions decreased organic matter remineralization and allowed the deposition of the Hg by organic-rich particles and accumulation in the sediments (Fig. 5). The CaCO3 (%) increase and positive values for the δ13C of C. wuellerstorfi (Fig. 4c and d) reinforce the hypothesis that the pattern of Hg for these periods was being influenced by deep-water changes such as changes in position, extent and/or physicochemical conditions of water masses in this region.

Unlike MIS 4, Hg concentrations in sediment were higher during the LGM/MIS 2 (Fig. 4a). Furthermore, it had the same pattern as $CaCO_3$ and TOC (Fig. 4b and c). Although εNd from TNO57-21(41,11 °S, 7,91 °E, water column depth 4981 m) and GeoB3808-6 (30.8° S, 14.7° W, 3213 m water depth) indicated the presence of corrosive southern-sourced waters during this period, the εNd isotope from GL-1090 had values ranging between −10 and −11 in the LGM (Fig. 4e) (Howe et al., 2016b, 2018). The high values were attributed to mixing from northern-sourced waters and southern-sourced water, where the intermediate depths were mostly filled by northern-sourced water (Howe et al., 2018). The increase in vertical mixing in the GL-1090 region allowed organic carbon preservation as well as carbonate precipitation. This could also explain the Hg accumulation during LGM/MIS 2 (Fig. 4a).

4.3. Paleoredox change and AMOC recovery in Termination II

The penultimate deglaciation is recognized by Termination II (T-II 129−135 ka) (Lourantou et al., 2010; Schneider et al., 2013), which included a reported rise of ~100 ppmv in atmospheric CO_2 (Fig. 6f) (Lourantou et al., 2010 Schneider et al., 2013). This abrupt increase in atmospheric CO_2 is linked to the enhancement of North Atlantic ventilation and vigorous strengthening of AMOC (Lourantou et al., 2010; Böhm et al., 2014; Deaney et al., 2017). After T-II, in early MIS 5e, Hg concentration in GL-1090 showed an abrupt increase reaching the highest value within the core (83.63 ng g^{-1}) (Fig. 6a) and decoupling from TOC (Fig. 6b and c). However, after 130 ka, Hg and organic carbon had the lowest concentrations between 129 and 126 ka (Fig. 6a and b). The opposite trend was observed in Mn and $CaCO_3$, with both having the highest values in the core (Fig. 6c and d).

The improvement of ventilation in the South Atlantic Ocean after T-II has been linked to the formation of an oxidation front in deep marine sediments. As a consequence, organic carbon originally supplied to the sediments was effectively degraded in a process referred to as burndown. (Thomson et al., 1990, 1996; Kasten et al., 2001; Wagner and Hendy, 2015). Evidence of this process includes the dramatic drop in the sedimentation rate followed by a decrease in organic carbon accumulation (Thomson et al., 1990, 1996; Kasten et al., 2001; Mangini et al., 2001; Wagner and Hendy, 2015). The sedimentation rate in GL-1090 dropped sharply (from 9 cm/kyr to 3 cm/kyr) at 130 ka, reaching the lowest value at 125 ka (2 cm/kyr) (Fig. 6b). The TOC record also decreased with the lowest value observed at ~127 ka (Fig. 6b). These findings are in agreement with other studies that proposed the same mechanism (Thomson et al., 1996; Mangini et al., 2001; Kasten et al., 2001; Wagner and Hendy, 2015), indicating the burndown processes occurred after

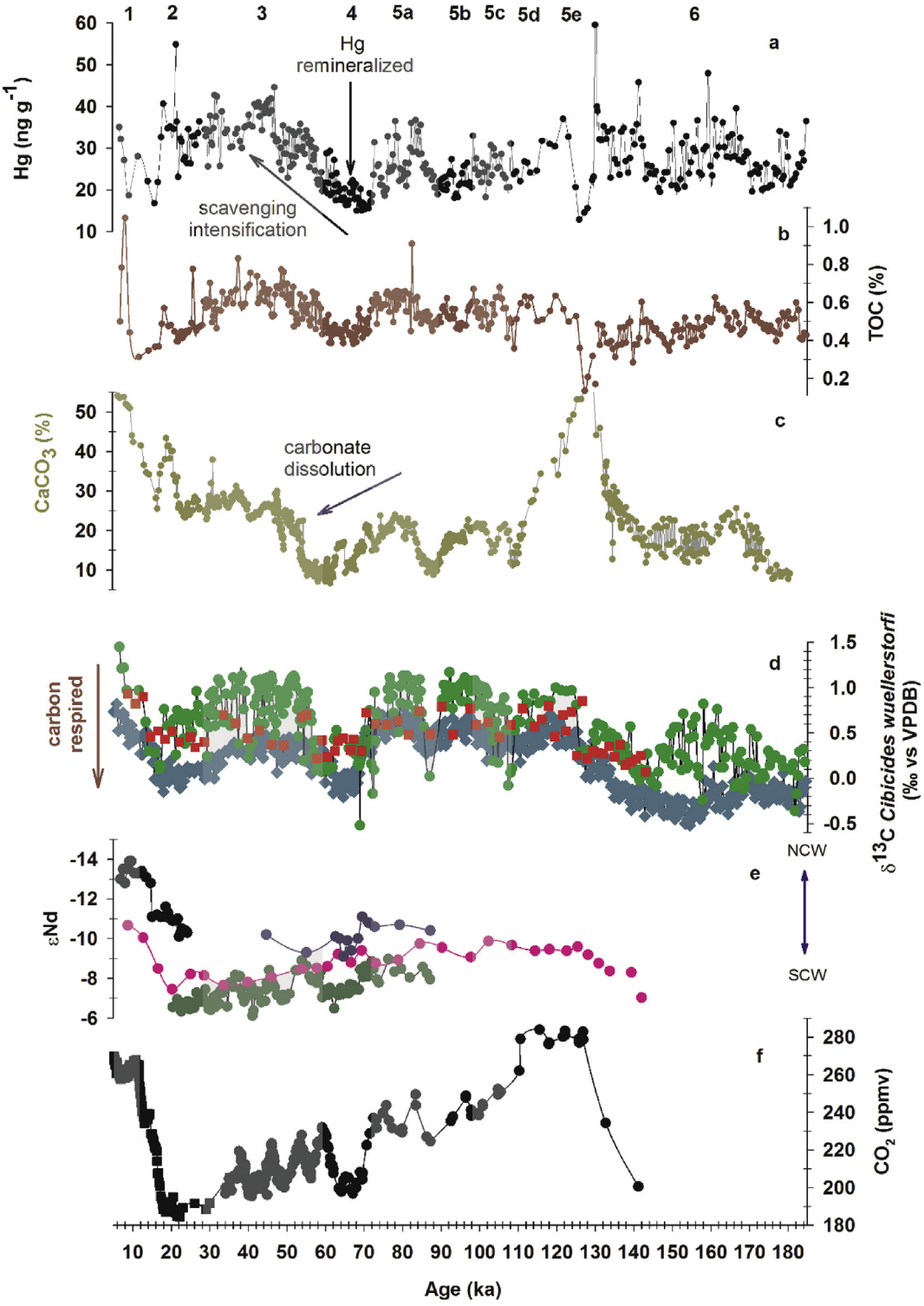

Fig. 4. Relationship between paleocirculation proxies and mercury geochemistry during the last 185 thousand years. Plot (a) mercury distribution in GL1090, plot (b) total organic carbon in GL1090, (c) CaCO3 in GL1090 (d) benthic δ13C compilation the light green circles correspond the values in Santos et al. (2017) to GL1090, dark green diamonds of the RC11-83 (40° 36′S, 9°48′E, water depth 4718 m)and red square of the GeoB2808-6 (30,8 °S, 14.7 °W, water depth, 3213 m) (Jonkers et al., 2015), plot (e) εNd data compilation, the dark green circles of the TNO57-21(41,11 °S, 7,91 °E, water depth 4981 m) (Piotrowski et al., 2005), the pink circles of the GeoB3808-6 (30.8° S, 14.7° W, 3213 m water depth) (Jonkers et al., 2015), dark blue circles of the MD99-2198 (12.09° N, 61.23°W; 1330 m water depth) (Griffiths et al., 2013) and the black circles of the GL-1090 core (24.92 °S, 42.51 °W, 2225 m water depth, 1914 cm long) (Howe et al., 2016a, b; Howe et al., 2018). (f) CO2 compilation from Antarctic cores (Bereiter et al., 2012; Eggleston et al., 2016). The light grey and white bars represent each MIS. (For interpretation of the references to colour in this figure legend, the reader is referred to the Web version of this article.)

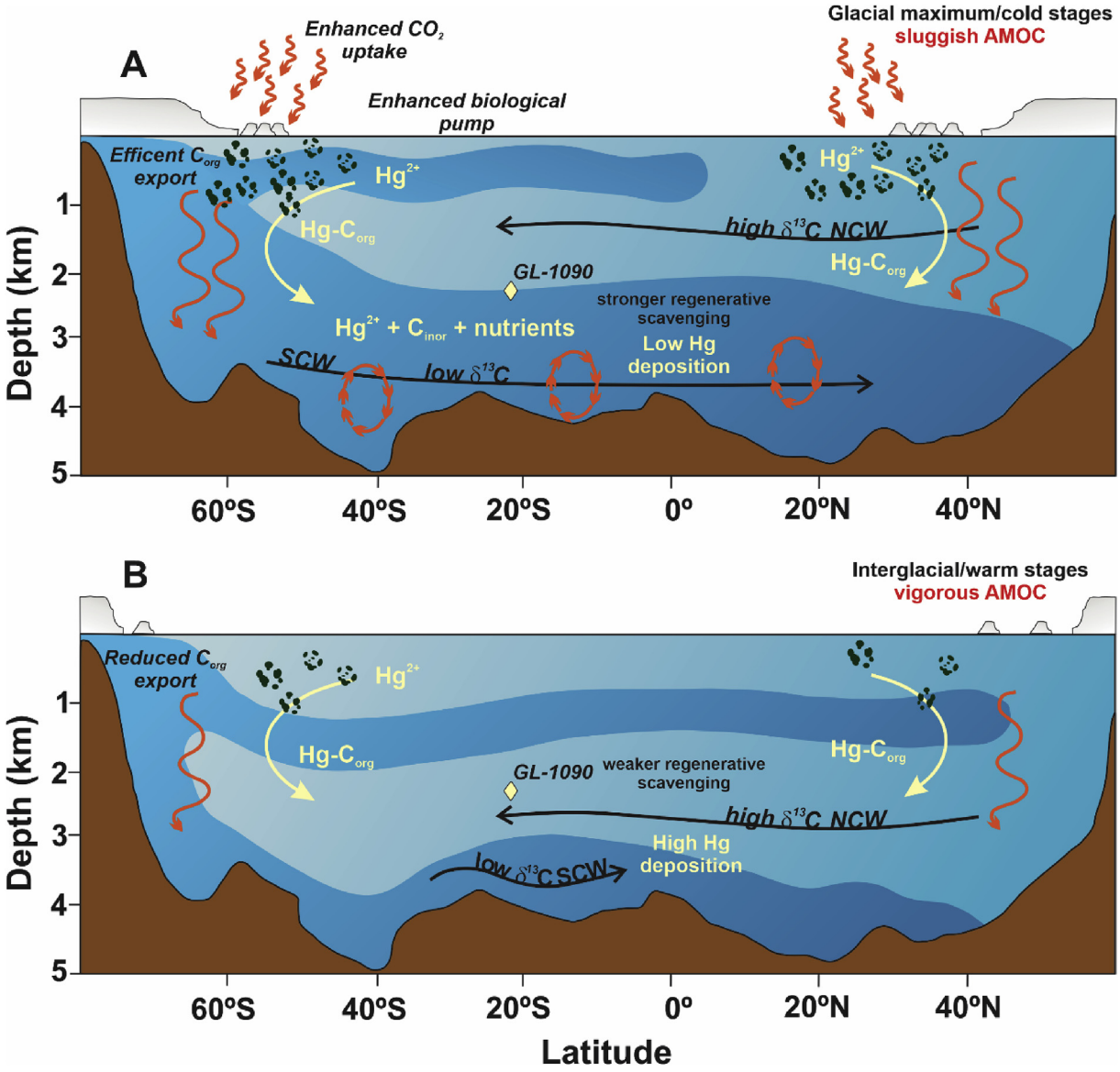

Fig. 5. Conceptual model showing the relationship between the biological pump and Hg cycle during glacial maximum/cold stages and interglacial/warm stages. In (A) glacial maximum/cold stages, it is characterized by intensification of regenerative scavenging of Hg. As a consequence, the water column beings more remineralized due to a more efficient biological pump, associated with weak and shoal AMOC, and the reduction in vertical mixing. In (B) interglacial/warm stages, a slowdown in Hg regenerative scavenging due to the resumption of NADW production is observed and, therefore, an increase of vertical mixing, decrease organic matter remineralization, greater removal of Hg to sediment.

T-II in the Southwestern Subtropical Atlantic as well.

To further support the burndown process, an increase in the oxygen content of the sediments in GL-1090 was examined through the $CaCO_3$ and Mn content (Fig. 4d and e). The geochemistry of Mn is dominated by the redox conditions, where Mn is oxidized and precipitates as insoluble Mn(III) and Mn(IV) oxides in oxygenated waters (Tribovillard et al., 2006). The Mn/Al ratio increased after T-II having an opposite trend as TOC and sedimentation rates (Fig. 6e), which supports higher preservation of Mn as oxidized solids. However, since Mn is also from lithogenic sources, changes in Mn may also be due to changes in lithogenic source regions. One way to assess changes in lithogenic source regions is the Ti/Al ratio (Muratli et al., 2010). The Ti/Al ratios exhibited a more significant oscillation within the T-II interval (Fig. 6e), while Mn/Al ratio was steady during the same period. This was followed by a rise of Mn/Al starting at 129 ka that reached the greatest values at ~125 ka, during which the Ti/Al did not exhibit significant variation (Fig. 6e). Therefore, the Mn record in the T-II interval in GL-1090 likely reflects the changes in bottom-water oxygen content. This hypothesis is reinforced by an increase of carbonate precipitation (Fig. 6d), which would be related to the presence of less corrosive northern-source waters indicating the resumption of the NADW formation (Sigman et al., 2010; Yu et al., 2016; Farmer et al., 2019) This result was in agreement with less radiogenic εNd from ODP 1063 (33° 41′N, 57° 37′W, water depth 4584 m) (Fig. 6f), (Deaney et al., 2017).

When organic matter is remineralized, it can cause the remobilization of reduced trace metals phases (Tribovillard et al., 2006). Once remobilized, trace metals can either diffuse downward into sediment column or diffuse upward out of sediment into the water column if concentration gradients decrease in those directions (Mangini et al., 2001; Tribovillard et al., 2006; Wagner and Hendy, 2015). According to Gagnon et al. (1997), the degradation of organic matter is one of the factors responsible for the release of inorganic Hg to the sediment porewaters. Utilizing this mechanism, after T-II

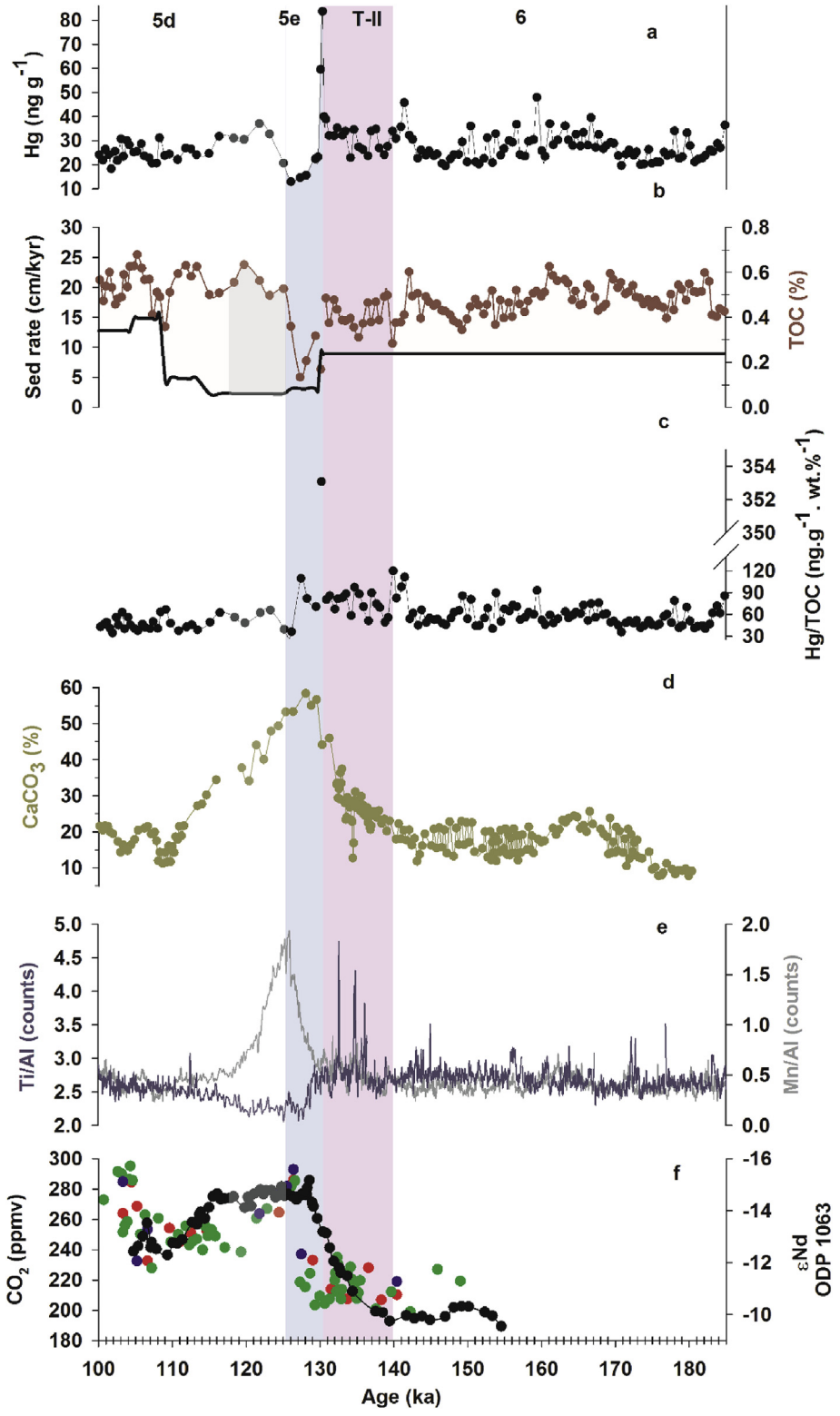

Fig. 6. Mercury and paleoenvironmental proxy distribution during T-II interval. Plot (a) Hg (ng.g^{-1}), plot (b) TOC (%) and sedimentation rates (cm/kyr), plot (c) Hg/TOC (%), plot (d) $CaCO_3$ (%), plot (e) Ti/Al ratio represented by the dark blue line and Mn/Al ration demonstrated by dark grey line, plot (f) CO_2 (ppmv) from EPICA Dome C (EDC) and Talos Dome represented by black circles (Schneider et al., 2013) and εNd from ODP 1063 (33° 41′N, 57° 37′W, water depth 4584 m) data represented by light green circle were obtained in Böhm et al. (2014), data represented by blue and red circles were obtained in Böhm et al. (2014) and Deaney et al. (2017). Purple bar illustrates the T-II interval, and the blue bar represents the oxidation front formation into fo MIS 5e. The light grey bar represents MIS 5e. (For interpretation of the references to colour in this figure legend, the reader is referred to the Web version of this article.)

(between 130 and 126 ka), the burndown of OM could have promoted the release, migration, and precipitation of Hg in other sediment layers, potentially explaining the Hg peak at the end of T-II.

In marine sediments, the mobility of Hg is affected by dissolution and precipitation of the several components of the solid sediment (Gobeil and Cossa, 1993; Gagnon et al., 1997; Fitzgerald et al., 2007). Processes such as the remineralization of organic matter, dissolution of authigenic and detrital Fe–Mn oxides, as well as the oxidation of iron sulfides are responsible for releasing inorganic Hg to the sediment porewaters (Gagnon et al., 1997). In anoxic sediment, Hg can be re-adsorbed onto residual organic matter or iron sulfides compounds, while in oxic layers, the adsorption occurs onto Fe–Mn oxides and fresh organic matter (Gobeil and Cossa, 1993; Gagnon et al., 1997). In the oxic/post-oxic boundary, Mercone et al. (1999) proposed the formation of HgSe (tiemmanite) after the release of ionic species into pore water followed by the oxidation of reduced Hg species. However, the results obtained for GL-1090 do not allow any inferences about the partitioning of Hg.

5. Conclusions

Over the last 185 ka, the total Hg concentration record from core GL-1090 indicated that Hg accumulation in South Atlantic Ocean deep-sea sediments during glacial stages was closely linked to the deep carbon cycle and directly related to the remineralization of organic carbon. The absence of correlations with major elemental ratios showed that terrestrial runoff had little to no influence on Hg input. Furthermore, the strong relationship between Hg and benthic $\delta^{13}C$ showed that the scavenging process of this metal responded to physical and chemical conditions imposed by NADW and a change in the position and extent of water masses promoted the accumulation of reactive species of this metal in deep-sea sediments as was observed in MIS 4. There was also the occurrence of an active oxic/post-oxic boundary due to increases in bottom ventilation at ~130-125 ka. This was associated with the AMOC recovery, which promoted efficient remineralization of organic matter and the redistribution of Hg within the solid phase. This conclusion was reinforced by an increase in the Mn signal and calcium carbonate precipitation. Therefore, this work provides strong evidence for the significant influence of global ocean circulation on Hg accumulation in deep-sea sediments.

Author statement

Thiago S. Figueiredo: conceptualization, writing - original draft. **Thiago P. Santos**: review, editing and software. **Karen B. Costa**: review. **Felipe Toledo**: review. **Ana Luiza S. Albuquerque**: writing, review and funding acquisition. **Joseph M. Smoak**: review and editing, **Bridget A. Bergquist**: review and editing. **Emmanoel Vieira Silva-Filho:** supervision**,** conceptualization writing, review-editing and funding acquisition.

Declaration of competing interest

The authors declare that they have no known competing financial interests or personal relationships that could have appeared to influence the work reported in this paper.

Acknowledgments

This study was financed in part by the Coordenação de Aperfeiçoamento de Pessoal de Nível Superior - Brasil (CAPES) - Finance Code 001. The authors are grateful for funding from CAPES-ASpECTO project (grant 88887.091731/2014-01) and PALEOCEANO-CAPES (23038.001417/2014e71). We thank R. Kowsman (CENPES/PETROBRAS) and PETROBRAS Core Repository staff (Macaé/PETROBRAS) for supplying the sediment used in this study. The authors are also grateful for the support of the CLIMATE-PRINT-UFF Project (grant CAPES 88887.310301/2018–00). E. Silva-Filho is senior researcher of the National Council for Research and Development (CNPq, Brazil) and the Foundation for Research Support of the State of Rio de Janeiro (FAPERJ E-26/203.037/2017). The data reported in this paper will be archived in Pangaea (www.pangaea.de)

Appendix A. Supplementary data

Supplementary data to this article can be found online at https://doi.org/10.1016/j.quascirev.2020.106368.

References

Amakawa, H., Tazoe, H., Obata, H., Gamo, T., Sano, Y., Shen, C.C., 2013. Neodymium isotopic composition and concentration in the southwest Pacific Ocean. Geochem. J. 47, 409–422. https://doi.org/10.2343/geochemj.2.0260.

Arz, H.W., Pätzold, J., Wefer, G., 1998. Correlated millennial-scale changes in surface hydrography and terrigenous sediment yield inferred from last-glacial marine deposits off northeastern Brazil. Quat. Res. 50, 157–166. https://doi.org/10.1006/qres.1998.1992.

Bereiter, B., Lüthi, D., Siegrist, M., Schüpbach, S., Stocker, T.F., Fischer, H., 2012. Mode change of millennial CO 2 variability during the last glacial cycle associated with a bipolar marine carbon seesaw. Proc. Natl. Acad. Sci. U.S.A. 109, 9755–9760. https://doi.org/10.1073/pnas.1204069109.

Blaauw, M., Christeny, J.A., 2011. Flexible paleoclimate age-depth models using an autoregressive gamma process. Bayesian Anal. 6, 457–474. https://doi.org/10.1214/11-BA618.

Böhm, E., Lippold, J., Gutjahr, M., Frank, M., Blaser, P., Antz, B., Fohlmeister, J., Frank, N., Andersen, M.B., Deininger, M., 2014. Strong and deep Atlantic meridional overturning circulation during the last glacial cycle. Nature 517, 73–76. https://doi.org/10.1038/nature14059.

Chaney, R.C., Slonim, S.M., Slonim, S.S., et al., 1982. Determination of calcium carbonate content in soils. In: Demars, K.R., Chaney, R.C. (Eds.), Geotechnical Properties, Behavior, and Performance of Calcareous Soils. American Society for Testing and Materials, pp. 3–15.

Cossa, D., Heimbürger, L.-E., Lannuzel, D., Rintoul, S.R., Butler, E.C.V., Bowie, A.R., Averty, B., Watson, R.J., Remenyi, T., 2011. Mercury in the Southern Ocean. Geochem. Cosmochim. Acta 75, 4037–4052. https://doi.org/10.1016/j.gca.2011.05.001.

Cossa, D., Heimbürger, L.E., Sonke, J.E., Planquette, H., Lherminier, P., García-Ibáñez, M.I., Pérez, F.F., Sarthou, G., 2018. Sources, cycling and transfer of mercury in the Labrador Sea (Geotraces-Geovide cruise). Mar. Chem. 198, 64–69. https://doi.org/10.1016/j.marchem.2017.11.006.

Costa, K.B., Cabarcos, E., Santarosa, A.C.A., Battaglin, B.B.F., Toledo, F.A.L., 2016. A multiproxy approach to the climate and marine productivity variations along MIS 5 in SE Brazil: a comparison between major components of calcareous nannofossil assemblages and geochemical records. Palaeogeogr. Palaeoclimatol. Palaeoecol. 449, 275–288. https://doi.org/10.1016/j.palaeo.2016.02.032.

Curry, W.B., Oppo, D.W., 2005. Glacial water mass geometry and the distribution of ?? 13C of ??CO2 in the western Atlantic Ocean. Paleoceanography 20, 1–12. https://doi.org/10.1029/2004PA001021.

Deaney, E.L., Barker, S., van de Flierdt, T., 2017. Timing and nature of AMOC recovery across Termination 2 and magnitude of deglacial CO2 change. Nat. Commun. 8, 14595. https://doi.org/10.1038/ncomms14595.

Dickson, R., Brown, J., 1994. The production of North Atlantic Deep Water : sources , rates , and pathways la . Worthington ' s scheme conversion paths North Circled numbers are transport estimates in Sverdrups , where lb . The recasting of Worthington ' s scheme by McCartney and. J. Geophys. Res. 99, 12,319-12,341.

Eggleston, S., Schmitt, J., Bereiter, B., Schneider, R., Fischer, H., 2016. Evolution of the Stable Carbon Isotope Composition of Atmospheric CO 2 over the Last Glacial Cycle 434–452. https://doi.org/10.1002/2015PA002874.Received.

Eide, M., Olsen, A., Ninnemann, U.S., Eldevik, T., 2017a. A global estimate of the full oceanic 13C Suess effect since the preindustrial. Global Biogeochem. Cycles 31, 492–514. https://doi.org/10.1002/2016GB005472.

Eide, M., Olsen, A., Ninnemann, U.S., Johannessen, T., 2017b. A global ocean climatology of preindustrial and modern ocean δ13C. Global Biogeochem. Cycles 31, 515–534. https://doi.org/10.1002/2016GB005473.

Fadina, O.A., Venancio, I.M., Belem, A., Silveira, C.S., Bertagnolli, D. de C., Silva-Filho, E.V., Albuquerque, A.L.S., 2019. Paleoclimatic controls on mercury deposition in northeast Brazil since the Last Interglacial. Quat. Sci. Rev. 221, 105869. https://doi.org/10.1016/j.quascirev.2019.105869.

Farmer, J.R., Hönisch, B., Haynes, L.L., Kroon, D., Jung, S., Ford, H.L., Raymo, M.E., Jaume-Seguí, M., Bell, D.B., Goldstein, S.L., Pena, L.D., Yehudai, M., Kim, J., 2019. Deep Atlantic Ocean carbon storage and the rise of 100,000-year glacial cycles. Nat. Geosci. 12, 355–360. https://doi.org/10.1038/s41561-019-0334-6.

Fitzgerald, W.F., Lamborg, C.H., Hammerschmidt, C.R., 2007. Marine Biogeochemical

Cycling of Mercury. Public Health.
Frank, M., 2002. Radiogenic isotopes: tracers of past ocean circulation and erosional input. Rev. Geophys. 40 https://doi.org/10.1029/2000RG000094, 1-1-1–38.
Gagnon, C., Pelletier, É., Mucci, A., 1997. Behaviour of anthropogenic mercury in coastal marine sediments. Mar. Chem. 59, 159–176. https://doi.org/10.1016/S0304-4203(97)00071-6.
Gebbie, G., 2014. How much did glacial North Atlantic water shoal? Paleoceanography 29, 190–209. https://doi.org/10.1002/2013PA002557.
Gehrke, G.E., Blum, J.D., Meyers, P.a., 2009. The geochemical behavior and isotopic composition of Hg in a mid-Pleistocene western Mediterranean sapropel. Geochem. Cosmochim. Acta 73, 1651–1665. https://doi.org/10.1016/j.gca.2008.12.012.
Gobeil, C., Cossa, D., 1993. Mercury in sediments and sediment pore water in the Laurentian Trough. Can. J. Fish. Aquat. Sci. 50, 1794–1800. https://doi.org/10.1139/f93-201.
Govin, Aline, Holzwarth, Ulrike, Heslop, David, Keeling F, Lara, Zabel, Matthias, Mulitza, Stefan, Collins A, James, Chiessi M, Cristiano, 2012. Distribution of major elements in Atlantic surface sediments (36°N–49°S): Imprint of terrigenous input and continental weathering. Geochem. Geophys. Geosys.
Govin, A., Michel, E., Labeyrie, L., Waelbroeck, C., Dewilde, F., Jansen, E., 2009. Evidence for northward expansion of Antarctic Bottom Water mass in the Southern Ocean during the last glacial inception. Paleoceanography 24, 1–14. https://doi.org/10.1029/2008PA001603.
Govin, A., Chiessi, C.M., Zabel, M., Sawakuchi, A.O., Heslop, D., Hörner, T., Zhang, Y., Mulitza, S., 2014. Terrigenous input off northern South America driven by changes in Amazonian climate and the North Brazil Current retroflection during the last 250 ka. Clim. Past 10, 843–862. https://doi.org/10.5194/cp-10-843-2014.
Grasby, S.E., Sanei, H., Beauchamp, B., Chen, Z., 2013a. Mercury deposition through the permo-triassic biotic crisis. Chem. Geol. 351, 209–216. https://doi.org/10.1016/j.chemgeo.2013.05.022.
Grasby, S.E., Sanei, H., Beauchamp, B., Chen, Z., 2013b. Mercury deposition through the permo–triassic biotic crisis. Chem. Geol. 351, 209–216. https://doi.org/10.1016/j.chemgeo.2013.05.022.
Grasby, S.E., Shen, W., Yin, R., Gleason, J.D., Blum, J.D., Lepak, R.F., Hurley, J.P., Beauchamp, B., 2017. Isotopic signatures of mercury contamination in latest Permian oceans. Geology 45, 55–58. https://doi.org/10.1130/G38487.1.
Griffiths, J.D., Barker, S., Hendry, K.R., Thornalley, D.J.R., Van De Flierdt, T., Hall, I.R., Anderson, R.F., 2013. Evidence of silicic acid leakage to the tropical atlantic via antarctic intermediate water during marine isotope stage 4. Paleoceanography 28, 307–318. https://doi.org/10.1002/palo.20030.
Gutjahr, M., Hoogakker, B.A.A., Frank, M., McCave, I.N., 2010. Changes in north atlantic deep water strength and bottom water masses during marine isotope stage 3 (45-35kaBP). Quat. Sci. Rev. 29, 2451–2461. https://doi.org/10.1016/j.quascirev.2010.02.024.
Henry, L.G., McManus, J.F., Curry, W.B., Roberts, N.L., Piotrowski, A.M., Keigwin, L.D., 2016. North Atlantic ocean circulation and abrupt climate change during the last glaciation. Paleoceanography 353, 470–474.
Hessler, I., Steinke, S., Groeneveld, J., Dupont, L., Wefer, G., 2011. Impact of abrupt climate change in the tropical southeast Atlantic during Marine Isotope Stage (MIS) 3. Paleoceanography 26, 1–11. https://doi.org/10.1029/2011PA002118.
Howe, J.N.W., Piotrowski, A.M., Oppo, D.W., Huang, K.F., Mulitza, S., Chiessi, C.M., Blusztajn, J., 2016a. Antarctic intermediate water circulation in the South Atlantic over the past 25,000 years. Paleoceanography 31, 1302–1314. https://doi.org/10.1002/2016PA002975.
Howe, J.N.W., Piotrowski, A.M., Noble, T.L., Mulitza, S., Chiessi, C.M., Bayon, G., 2016b. North Atlantic deep water production during the last glacial maximum. Nat. Commun. 7, 11765. https://doi.org/10.1038/ncomms11765.
Howe, J.N.W., Huang, K.-F., Oppo, D.W., Chiessi, C.M., Mulitza, S., Blusztajn, J., Piotrowski, A.M., 2018. Similar mid-depth atlantic water mass provenance during the last glacial maximum and heinrich stadial 1. Earth Planet Sci. Lett. 490, 51–61. https://doi.org/10.1016/j.epsl.2018.03.006.
Jaccard, S.L., Galbraith, E.D., Martínez-Garciá, A., Anderson, R.F., 2016. Covariation of deep Southern Ocean oxygenation and atmospheric CO2through the last ice age. Nature 530, 207–210. https://doi.org/10.1038/nature16514.
Jitaru, P., Gabrielli, P., Marteel, A., Plane, J.M.C., Planchon, F.A.M., Gauchard, P.A., Ferrari, C.P., Boutron, C.F., Adams, F.C., Hong, S., Cescon, P., Barbante, C., 2009. Atmospheric depletion of mercury over Antarctica during glacial periods. Nat. Geosci. 2, 505–508. https://doi.org/10.1038/ngeo549.
Johnson, G.C., 2008. Quantifying antarctic bottom water and north atlantic deep water volumes. J. Geophys. Res. Ocean. 113, 1–13. https://doi.org/10.1029/2007JC004477.
Jonkers, L., Zahn, R., Thomas, A., Henderson, G., Abouchami, W., Franois, R., Masque, P., Hall, I.R., Bickert, T., 2015. Deep circulation changes in the central South Atlantic during the past 145 kyrs reflected in a combined 231Pa/230Th, Neodymium isotope and benthic ??C13 record. Earth Planet Sci. Lett. 419, 14–21. https://doi.org/10.1016/j.epsl.2015.03.004.
Kasten, S., Haese, R.R., Zabel, M., Rühlemann, C., Schulz, H.D., 2001. Barium peaks at glacial terminations in sediments of the equatorial Atlantic Ocean—relicts of deglacial productivity pulses? Chem. Geol. 175, 635–651. https://doi.org/10.1016/S0009-2541(00)00377-6.
Kissel, C., Laj, C., Labeyrie, L., Dokken, T., Voelker, A., Blamart, D., 1999. Rapid climate variations during marine isotope stage 3: magnetic analysis of sediments from Nordic Seas and Atlantic. Earth Planet Sci. Lett. 171, 489–502.
Kita, I., Kojima, M., Hasegawa, H., Chiyonobu, S., Sato, T., 2013. Mercury content as a new indicator of ocean stratification and primary productivity in Quaternary sediments off Bahama Bank in the Caribbean Sea. Quat. Res. 4–11. https://doi.org/10.1016/j.yqres.2013.08.006.
Lacerda, L.D., Turcq, B., Sifeddine, A., Cordeiro, R.C., 2017. Mercury accumulation rates in Caço Lake, NE Brazil during the past 20.000 years. J. South Am. Earth Sci. 77, 42–50. https://doi.org/10.1016/j.jsames.2017.04.008.
Lamborg, C.H., Hammerschmidt, C.R., Bowman, K.L., Swarr, G.J., Munson, K.M., Ohnemus, D.C., Lam, P.J., Heimbürger, L.-E., Rijkenberg, M.J.A., Saito, M.A., 2014. A global ocean inventory of anthropogenic mercury based on water column measurements. Nature 512, 65–68. https://doi.org/10.1038/nature13563.
Lambert, F., Delmonte, B., Petit, J.R., Bigler, M., Kaufmann, P.R., Hutterli, M.A., Stocker, T.F., Ruth, U., Steffensen, J.P., Maggi, V., et al., 2008. Dust-climate couplings over the past 800,000 years from the EPICA Dome C ice core. Nature. https://doi.org/10.1038/nature06763.
Lamborg, C.H., Hammerschmidt, C.R., Bowman, K.L., 2016. An examination of the role of particles in oceanic mercury cycling. Philos. Trans. R. Soc. A Math. Phys. Eng. Sci. 374, 20150297. https://doi.org/10.1098/rsta.2015.0297.
Laurier, F.J.G., Mason, R.P., Gill, G.a., Whalin, L., 2004. Mercury distributions in the north Pacific Ocean—20 years of observations. Mar. Chem. 90, 3–19. https://doi.org/10.1016/j.marchem.2004.02.025.
Lessa, D.V.O., Santos, T.P., Venancio, I.M., Albuquerque, A.L.S., 2017. Offshore expansion of the Brazilian coastal upwelling zones during Marine Isotope Stage 5. Global Planet. Change 158, 13–20. https://doi.org/10.1016/j.gloplacha.2017.09.006.
Lippold, J., Luo, Y., Francois, R., Allen, S.E., Gherardi, J., Pichat, S., Hickey, B., Schulz, H., 2012. Strength and geometry of the glacial atlantic meridional overturning circulation. Nat. Geosci. 5, 813–816. https://doi.org/10.1038/ngeo1608.
Lisiecki, L.E., Raymo, M.E., 2005. A Pliocene-Pleistocene stack of 57 globally distributed benthic δ 18O records. Paleoceanography 20, 1–17. https://doi.org/10.1029/2004PA001071.
Lourantou, A., Chappellaz, J., Barnola, J.M., Masson-Delmotte, V., Raynaud, D., 2010. Changes in atmospheric CO2 and its carbon isotopic ratio during the penultimate deglaciation. Quat. Sci. Rev. 29, 1983–1992. https://doi.org/10.1016/j.quascirev.2010.05.002.
Lund, D.C., Adkins, J.F., Ferrari, R., 2011. Abyssal atlantic circulation during the last glacial maximum: constraining the ratio between transport and vertical mixing. Paleoceanography 26, 1–19. https://doi.org/10.1029/2010PA001938.
Mahiques, M.M., Tassinari, C.C.G., Marcolini, S., Violante, R.A., Figueira, R.C.L., da Silveira, I.C.A., Burone, L., de Mello e Sousa, S.H., 2008. Nd and Pb isotope signatures on the Southeastern South American upper margin: implications for sediment transport and source rocks. Mar. Geol. 250, 51–63. https://doi.org/10.1016/j.margeo.2007.11.007.
Mangini, A., Jung, M., Laukenmann, S., 2001. What do we learn from peaks of uranium and of manganese in deep sea sediments? Mar. Geol. 177, 63. https://doi.org/10.1016/S0025-3227(01)00124-4.
Martinez-Cortizas, A., Pontevedra-Pombal, X., García-Rodeja, E., Nóvoa-Muñoz, J., Shotyk, W., 1999. Mercury in a Spanish peat bog: archive of climate change and atmospheric metal deposition. Science (80-.) 284, 939–942. https://doi.org/10.1126/science.284.5416.939.
Mason, R.P., Fitzgerald, W.F., 1991. Mercury speciation in open ocean waters. Water Air Soil Pollut. 56, 779–789. https://doi.org/10.1007/BF00342316.
Mason, R.P., Reinfelder, J.R., 1996. Uptake , toxicity , and trophic transfer of mercury in a coastal diatom. Environ. Sci. Technol. 30, 1835–1845.
Mason, R.P., Sullivan, K.A., 1999. The distribution and speciation of mercury in the South and equatorial Atlantic. Deep. Res. 46, 937–956.
Mason, R., Rolfhus, K., Fitzgerald, W., 1998. Mercury in the north atlantic. Mar. Chem. 61, 37–53.
Mason, R.P., Choi, A.L., Fitzgerald, W.F., Hammerschmidt, C.R., Lamborg, C.H., Soerensen, A.L., Sunderland, E.M., 2012. Mercury biogeochemical cycling in the ocean and policy implications. Environ. Res. 1–17 https://doi.org/10.1016/j.envres.2012.03.013.
Mémery, L., Arhan, M., Alvarez-Salgado, X.A., Messias, M.J., Mercier, H., Castro, C.G., Rios, A.F., 2000. The water masses along the western boundary of the south and equatorial Atlantic. Prog. Oceanogr. 47, 69–98. https://doi.org/10.1016/S0079-6611(00)00032-X.
Mercone, D., Thomson, J., Croudace, I.W., Troelstra, S.R., 1999. A coupled natural immobilsation mechanism for mercury and selenium in deep-sea sediments. Geochem. Cosmochim. Acta 63, 1481–1488. https://doi.org/10.1016/s0016-7037(99)00063-0.
Muratli, J.M., Chase, Z., Mix, A.C., McManus, J., 2010. Increased glacial-age ventilation of the Chilean margin by antarctic intermediate water. Nat. Geosci. 3, 23–26. https://doi.org/10.1038/ngeo715.
Negre, C., Zahn, R., Thomas, A.L., Masqué, P., Henderson, G.M., Martínez-Méndez, G., Hall, I.R., Mas, J.L., 2010. Reversed flow of atlantic deep water during the last glacial maximum. Nature 468, 84–88. https://doi.org/10.1038/nature09508.
Pearce, C.R., Jones, M.T., Oelkers, E.H., Pradoux, C., Jeandel, C., 2013. The effect of particulate dissolution on the neodymium (Nd) isotope and Rare Earth Element (REE) composition of seawater. Earth Planet Sci. Lett. 369–370, 138–147. https://doi.org/10.1016/j.epsl.2013.03.023.
Perez, L., García-Rodríguez, F., Hanebuth, T.J.J., 2016. Variability in terrigenous sediment supply offshore of the Río de la Plata (Uruguay) recording the continental climatic history over the past 1200 years. Clim. Past 12, 623–634. https://doi.org/10.5194/cp-12-623-2016.
Peterson, R.G., Stramma, L., 1991. Upper-level circulation in the south Atlantic

Ocean. Prog. Oceanogr. 26, 1–73. https://doi.org/10.1016/0079-6611(91)90006-8.
Piepgras, D.J., Wasserburg, G.J., 1982. Isotopic composition of neodymium in waters from the Drake passage. Science (80- 217, 207–214. https://doi.org/10.1126/science.217.4556.207.
Piotrowski, A.M., Goldstein, S.L., Hemming, S.R., Fairbanks, R.G., 2005. Temporal relationship of carbon cycling and ocean circulation at glacial boundaries. Science 80 (307), 1933–1938. https://doi.org/10.1126/science.1104883.
Piotrowski, A.M., Goldstein, S.L., Hemming, S.R., Fairbanks, R.G., Zylberberg, D.R., 2008. Oscillating glacial northern and southern deep water formation from combined neodymium and carbon isotopes. Earth Planet Sci. Lett. 272, 394–405. https://doi.org/10.1016/j.epsl.2008.05.011.
Portilho-Ramos, R. da C., Ferreira, F., Calado, L., Frontalini, F., de Toledo, M.B., 2015. Variability of the upwelling system in the southeastern Brazilian margin for the last 110,000 years. Global Planet. Change 135, 179–189. https://doi.org/10.1016/j.gloplacha.2015.11.003.
Rasmussen, T.L., Thomsen, E., Moros, M., 2016. North Atlantic warming during Dansgaard-Oeschger events synchronous with Antarctic warming and out-of-phase with Greenland climate. Sci. Rep. 6, 1–12. https://doi.org/10.1038/srep20535.
Ravichandran, M., 2004. Interactions between mercury and dissolved organic matter - a review. Chemosphere 55, 319–331. https://doi.org/10.1016/j.chemosphere.2003.11.011.
Sanei, H., Grasby, S.E., Beauchamp, B., 2012. Latest permian mercury anomalies. Geology 40, 63–66. https://doi.org/10.1130/G32596.1.
Santos, T.P., Lessa, D.O., Venancio, I.M., Chiessi, C.M., Mulitza, S., Kuhnert, H., Govin, A., Machado, T., Costa, K.B., Toledo, F., Dias, B.B., Albuquerque, A.L.S., 2017. Prolonged warming of the Brazil Current precedes deglaciations. Earth Planet Sci. Lett. https://doi.org/10.1016/j.epsl.2017.01.014.
Schneider, R., Schmitt, J., Köhler, P., Joos, F., Fischer, H., 2013. A reconstruction of atmospheric carbon dioxide and its stable carbon isotopic composition from the penultimate glacial maximum to the last glacial inception. Clim. Past 9, 2507–2523. https://doi.org/10.5194/cp-9-2507-2013.
Sholupov, S., Pogarev, S., Ryzhov, V., Mashyanov, N., Stroganov, A., 2004. Zeeman atomic absorption spectrometer RA-915+ for direct determination of mercury in air and complex matrix samples. Fuel Process. Technol. 85, 473–485. https://doi.org/10.1016/j.fuproc.2003.11.003.
Sigman, D.M., Hain, M.P., Haug, G.H., 2010. The polar ocean and glacial cycles in atmospheric CO2 concentration. Nature 466, 47–55. https://doi.org/10.1038/nature09149.
Skinner, L.C., Waelbroeck, C., Scrivner, A.E., Fallon, S.J., 2014. Radiocarbon evidence for alternating northern and southern sources of ventilation of the deep Atlantic carbon pool during the last deglaciation. Proc. Natl. Acad. Sci. U.S.A. 111, 5480–5484. https://doi.org/10.1073/pnas.1400668111.
Soerensen, A.L., Sunderland, E.M., Holmes, C.D., Jacob, D.J., Yantosca, R.M., Skov, H., Christensen, J.H., Strode, S. a, Mason, R.P., 2010. An improved global model for air-sea exchange of mercury: high concentrations over the North Atlantic. Environ. Sci. Technol. 44, 8574–8580. https://doi.org/10.1021/es102032g.
Stramma, L., 1991. Geostrophic transport of the south equatorial current in the atlantic. J. Mar. Res. 49, 281–294. https://doi.org/10.1357/002224091784995864.
Stramma, L., England, M., 1999. On the water masses and mean circulation of the South Atlantic Ocean. J. Geophys. Res. Ocean. 104, 20863–20883. https://doi.org/10.1029/1999JC900139.
Talley, L.D., 1996. Antarctic intermediate water in the south atlantic. In: The South Atlantic. Springer Berlin Heidelberg, Berlin, Heidelberg, pp. 219–238. https://doi.org/10.1007/978-3-642-80353-6_11.
Tessin, A.C., Lund, D.C., 2013. Isotopically depleted carbon in the mid-depth South Atlantic during the last deglaciation. Paleoceanography 28, 296–306. https://doi.org/10.1002/palo.20026.
Thomson, J., Wallace, H.E., Colley, S., Toole, J., 1990. Authigenic uranium in Atlantic sediments of the last glacial stage - a diagenetic phenomenon. Earth Planet Sci. Lett. 98, 222–232. https://doi.org/10.1016/0012-821X(90)90061-2.
Thomson, J., Higgs, N.C., Colley, S., 1996. Diagenetic redistributions of redox-sensitive elements in northeast Atlantic glacial/interglacial transition sediments. Earth Planet Sci. Lett. 139, 365–377. https://doi.org/10.1016/0012-821X(96)00031-3.
Tribovillard, N., Algeo, T.J., Lyons, T., Riboulleau, A., 2006. Trace metals as paleoredox and paleoproductivity proxies: an update. Chem. Geol. 232, 12–32. https://doi.org/10.1016/j.chemgeo.2006.02.012.
Vandal, G.M., Fitzgerald, W.F., Boutron, C.F., Candelone, J.-P., 1993. Variations in mercury deposition to Antarctica over the past 34,000 years. Nature. https://doi.org/10.1038/362621a0.
Venancio, I.M., Mulitza, S., Govin, A., Santos, T.P., Lessa, D.O., Albuquerque, A.L.S., Chiessi, C.M., Tiedemann, R., Vahlenkamp, M., Bickert, T., Schulz, M., 2018. Millennial- to orbital-scale responses of western equatorial atlantic thermocline depth to changes in the trade wind system since the last interglacial. Paleoceanogr. Paleoclimatol. 33, 1490–1507. https://doi.org/10.1029/2018PA003437.
Wagner, M., Hendy, I.L., 2015. Trace metal evidence for a poorly ventilated glacial Southern Ocean. Clim. Past Discuss 11, 637–670. https://doi.org/10.5194/cpd-11-637-2015.
Yu, J., Menviel, L., Jin, Z.D., Thornalley, D.J.R., Barker, S., Marino, G., Rohling, E.J., Cai, Y., Zhang, F., Wang, X., Dai, Y., Chen, P., Broecker, W.S., 2016. Sequestration of carbon in the deep Atlantic during the last glaciation. Nat. Geosci. 9, 319–324. https://doi.org/10.1038/ngeo2657.
Zhang, Y., Jaeglé, L., Thompson, L., 2014. Natural biogeochemical cycle of mercury in a global three-dimensional ocean tracer model. Global Biogeochem. Cycles 28, 553–570. https://doi.org/10.1002/2014GB004814.
Ziegler, M., Diz, P., Hall, I.R., Zahn, R., 2013. Millennial-scale changes in atmospheric CO2 levels linked to the Southern Ocean carbon isotope gradient and dust flux. Nat. Geosci. 6, 457–461. https://doi.org/10.1038/ngeo1782.